Compression Artifact Reduction by Overlapped-Block Transform Coefficient Estimation with Block Similarity

Xinfeng Zhang, Ruiqin Xiong, *Member, IEEE*, Xiaopeng Fan, *Member*, *IEEE*, Siwei Ma, *Member, IEEE*, Wen Gao, *Fellow, IEEE*

***Abstract*—Block transform coded images usually suffer from annoying artifacts at low bit rates, caused by the coarse quantization of transform coefficients. In this paper, we propose a new method to reduce compression artifacts by overlapped-block transform coefficient estimation from non-local blocks. In the proposed method, the DCT coefficients of each block are estimated by adaptively fusing two prediction values based on their reliabilities. One prediction is the quantized values of coefficients decoded from the compressed bitstream, whose reliability is determined by quantization steps. The other prediction is the weighted average of coefficients in non-local blocks, whose reliability depends on the variance of coefficients in these blocks. The weights are utilized to distinguish the effectiveness of coefficients in non-local blocks to predict original coefficients and are determined by block similarity in transform domain. To solve the optimization problem, the overlapped blocks are divided into several subsets. Each subset contains non-overlapped blocks covering the whole image and is optimized independently. Therefore, the overall optimization is reduced to a set of sub-optimization problems, which can be easily solved. Finally, we provide a strategy for parameter selection based on the compression levels. Experimental results show that the proposed method can remarkably reduce compression artifacts and significantly improve both the subjective and the objective quality of block transform coded images.**

***Index Terms*—Block transform coding, compression artifacts, block similarity, denoising, post-processing**

Manuscript received September 12, 2012; revised January 17, 2013 and April 12, 2013. This work was supported in part by the National Basic Research Program of China (973 Program) under Grant 2009CB320904, the National Natural Science Foundation of China under Grants 61073083, 61121002 and 61103088, the Beijing Natural Science Foundation under Grants 4112026 and 4132039, and the Research Fund for the Doctoral Program of Higher Education under Grants 20100001120027 and 20120001110090. Copyright (c) 2013 IEEE. Personal use of this material is permitted. However, permission to use this material for any other purposes must be obtained from the IEEE by sending a request to pubs-permissions@ieee.org. The associate editor coordinating the review of this manuscript and approving it for publication was Prof. Sina Farsiu.

Xinfeng Zhang is with the Key Lab of Intelligent Information Processing, Institute of Computing Technology, Chinese Academy of Sciences, Beijing 100190, China and also with the University of Chinese Academy of Sciences, Beijing, 100049, China. He is also with the Institute of Digital Media, School of Electronic Engineering and Computer Science, Peking University, Beijing 100871, China (e-mail: xfzhang@jdl.ac.cn).

R. Xiong, S. Ma and W. Gao are with the Institute of Digital Media, School of Electronic Engineering and Computer Science, Peking University, Beijing 100871, China (e-mail: {rqxiong, swma, wgao}@pku.edu.cn).

X. Fan is with the Department of Computer Science, Harbin Institute of Technology (HIT), Harbin 150001, China (e-mail: fxp@hit.edu.cn).

I. Introduction

DISCRETE cosine transform (DCT) is widely adopted in the existing image and video compression standards, such as JPEG, MPEG-1/2/4, H.261/263/264, *etc.*, to exploit the spatial correlation among neighboring pixels. At the encoder of such schemes, the input image is usually divided into a group of small image blocks, each of which is transformed into the frequency domain using block-DCT (BDCT). For each transformed block, the DCT coefficients are then compressed into a binary stream via quantization and entropy coding. At the decoder, the image is reconstructed by inversely transforming the quantized DCT coefficients extracted from the bitstream. A problem in block transform coding is that, due to the coarse quantization of transform coefficients, the images compressed at low bit rate usually suffer from visually annoying artifacts [1], including the blocking and ringing effects.

In order to reduce the compression artifacts while maintaining compatibility with the existing coding standards, various post-processing techniques have been proposed in the literatures. These methods mainly include filtering approaches [2]-[6], iterative approaches based on the theory of *projections onto convex sets* (POCS) [7], [8], maximum *a posteriori* (MAP) estimation methods [9], [10] and wavelet-based methods [11]. Reeve and Lim [2] applied a 3×3 Gaussian filter to the pixels around block boundaries to smooth out the blocking artifacts. Ramamurthi and Gersho [3] employed nonlinear space-variant filters based on edge-oriented classifiers to smooth out blocking artifacts. Buades *et al*. [4], [5] proposed the nonlocal means filter to predict each pixel by a weighted average of its surrounding pixels, where the weights are determined by the similarity of the corresponding image patches located at the source and target coordinates. Takeda *et al*. [6] proposed a signal-dependent steering kernel regression framework for denoising. The above methods only considered the smoothness or the regularity in pixel intensities, but did not exploit the information in the compressed bitstream. Therefore, the true edges or texture details might be smoothed out undesirably in the reconstructed images. To avoid this issue, Zakhor *et al*. [7], [8] utilized the quantization intervals of transform coefficients as a convex set, resulting in an algorithm which applies low pass filtering and projection onto quantization convex set alternately. There are also many approaches based on probability estimation [9], [10]. Rourke and Stevenson [9] employed Huber-Markov random field (Huber-MRF) as an image prior model to seek the MAP estimation of the original image. The Gibbs distribution therein models both the

smoothness and the discontinuities of images in the spatial domain. Sun and Cham [10] modeled the original image as a high order Markov random field (MRF) based on the field of experts (FoE) framework. In some other approaches, the *a priori* knowledge is expressed by the statistical characteristics of coefficients in transform domain, *e.g.* wavelet, contourlet. Wu *et al*. [11] proposed a deblocking algorithm by adaptively shrinking the wavelet coefficients.

Since the compression artifacts are solely caused by the quantization of transform coefficients, some previous works tackle the problem in the DCT domain [12]-[16]. Chen *et al*. [12] applied a low pass filter to the DCT coefficients of neighboring blocks. The DCT-domain filtering method was also adopted in [13]. Although the filter was adaptively chosen, it remains constant with respect to all subbands. Therefore, the filtering operation in DCT domain is essentially equivalent to the corresponding filter in spatial domain. Choy *et al*. [14] estimates the original DCT coefficients from the quantized ones with the local mean and variance of the coefficients in each subband. Lee *et al*. [15] proposed to reduce artifacts by first low pass filtering the decoded image and then predicting the image by a linear regression model in transform domain. Foi *et al*. [16] utilized a point wise shape adaptive DCT for denoising.

In this paper, we propose a new approach to reduce compression artifacts by estimating the original image from transform domain. This is achieved by estimating the DCT coefficients in all the transform-blocks located at any pixel position. For each block, the DCT coefficients are estimated by adaptively fusing two prediction values according to their reliabilities. One prediction is the quantized values of coefficients decoded from the compressed bitstream, whose reliability is determined by quantization steps. The other prediction is the weighted average of coefficients in non-local blocks which are similar with the estimated blocks. Its reliability depends on the variance of coefficients in these similar blocks. The weights are utilized to distinguish the effectiveness of coefficients in similar blocks to predict the original coefficients. They are determined by block similarity in transform domain. In order to depress the negative effects of noise in similarity calculation, we take the Euclidean Distance of low frequency coefficients in transform-blocks to measure their similarities. Furthermore, we employ quantization steps to exclude outlier coefficients in similar blocks, which are far away from the estimated original coefficients. The proposed framework needs to optimize transform coefficients in all the transform-blocks in image, which are overlapped. It involves a large set of dependent variables. To tackle the optimization problem, the overlapped blocks are divided into several subsets. Each subset contains non-overlapped blocks covering the whole image and is optimized independently. Therefore, the overall optimization is reduced to a set of sub-optimization problems that can be easily solved. A method is also proposed to enforce the quantization constraint for each of these sub-optimization problems. Finally, we provide a strategy for parameter selection according to the compression levels or quantization steps, which can be extracted from the compression bitstream.

The remainder of this paper is organized as follows. Section II briefly reviews block-transform image coding and introduces some notations. Section III formulates the compression artifact reduction as a MAP estimation problem under the Bayesian framework. The proposed image prior models are described in detail, and the performances of different prior models are compared in this section. Section IV describes the optimization solution of the proposed algorithm and the enforced quantization constraint method. Experimental results are reported in Section V, and Section VI concludes the paper.

II. Review of Block-Transform Image Coding

In this section, we briefly review a few concepts and notations in block transform image coding for the convenience of later discussion. Suppose we have an image $\mathcal{I}$ (a two-dimensional grid) of size $H\times W$, where $\mathcal{I}(i, j)$ denotes a pixel and the indices i and j are the coordinates in the vertical and the horizontal directions, respectively. Suppose that the size of block-DCT used for image coding is $N\times N$. We use $\mathcal{B}_{m,n}$ to denote an image block of size $N\times N$ in $\mathcal{I}$, with its top left pixel being $\mathcal{I}(m, n)$. To be specific, the pixels in this block are

$$\mathcal{B}_{m,n}(i, j) = \mathcal{I}(m + i, n + j), \quad i, j = 0, 1,\ldots, N\text{-}1. \tag{1}$$

For the block-DCT based image coding, the input image $\mathcal{I}$ is divided into a group of non-overlapped blocks of size $N\times N$. The data in each block is transformed, quantized and entropy coded into the compressed bitstream. We call these blocks *coding blocks*. Obviously, a block $\mathcal{B}_{m,n}$ is a *coding block* only when m and n are multiples of N. We define

$$\Omega_{\mathrm{CB}} = \{\mathcal{B}_{m,n} \mid m, n \equiv 0 \ (\mathrm{mod}\ N)\}. \tag{2}$$

The complete set of blocks in image $\mathcal{I}$ is defined as

$$\Omega = \{\mathcal{B}_{m,n} \mid 0 \le m < H - N, 0 \le n < W - N\}. \tag{3}$$

The blocks in Ω are obviously overlapped. The blocks in $\Omega_{\mathrm{NCB}}=\Omega\backslash\Omega_{\mathrm{CB}}$ are called *non-coding blocks*. Although the data in *non-coding blocks* are not directly acquired from the bistream by inverse transform and quantization, they can be retrieved from the bitstream when the image is reconstructed.

We use $\mathbf{x}$ to represent the original data (*i.e.* pixel intensity) of image $\mathcal{I}$ and use $\mathbf{x}_{\mathcal{B}}$ and $\mathbf{X}_{\mathcal{B}}$ to represent the data and the transform coefficients of a block $\mathcal{B}$, respectively. They are related by the block-DCT $\mathcal{T}$, $\mathbf{X}_{\mathcal{B}} = \mathcal{T}(\mathbf{x}_{\mathcal{B}})$, (inverse transform $\mathbf{x}_{\mathcal{B}}= \mathcal{T}^{-1}(\mathbf{X}_{\mathcal{B}})$). The transform coefficients in $\mathbf{X}_{\mathcal{B}}$ are quantized according to a quantization matrix Q of size $N\times N$.

$$\mathbf{Y}_{\mathcal{B}}(u,v) = \mathcal{Q}(\mathbf{X}_{\mathcal{B}}(u,v)). \tag{4}$$

$\mathbf{Y}_{\mathcal{B}}(u,v)$ is the reconstructed coefficients in the block $\mathcal{B}$. This is achieved by $\mathbf{I}_{\mathcal{B}}(u,v)=round(\mathbf{X}_{\mathcal{B}}(u,v)/Q(u,v))$ and $\mathbf{Y}_{\mathcal{B}}(u,v)=Q(u,v)\mathbf{I}_{\mathcal{B}}(u,v)$. Here, $\mathbf{I}_{\mathcal{B}}(u,v)$ is the index of the

quantization interval for the block $\mathcal{B}$ and $Q(u,v)$ is a quantization step.

III. Framework of Coefficient Estimation with Block Similarity

In a standard decoder, the image is reconstructed simply by inversely transforming the quantized coefficients for each *coding block*. In this paper, we seek a better image recovery from the view point of statistical inference. This is formulated as follows: given the quantized transform coefficients $\mathbf{Y}_{\mathcal{B}}$ for each *coding block* $\mathcal{B}\in\Omega_{\mathrm{CB}}$, find the image $\mathbf{x}$ which has the maximum *a posteriori* probability:

$$\hat{\mathbf{x}} = \underset{\mathbf{x}}{\operatorname{argmax}}\ \mathbf{Pr}\left(\mathbf{x}\,|\,\{\mathbf{Y}_{\mathcal{B}}\}_{\mathcal{B}\in\Omega_{\mathrm{CB}}}\right). \tag{5}$$

Based on the Bayesian rule, the problem can be reformulated as

$$\hat{\mathbf{x}} = \underset{\mathbf{x}}{\operatorname{argmax}}\ \mathbf{logPr}\left(\{\mathbf{Y}_{\mathcal{B}}\}_{\mathcal{B}\in\Omega_{\mathrm{CB}}}\middle|\mathbf{x}\right) + \mathbf{logPr}(\mathbf{x}). \tag{6}$$

Here, the first term in (6) is the likelihood and the second term is the prior model of image $\mathbf{x}$. In the literatures, many image prior models have been proposed (*e.g.* [17]-[20]). In this paper, we propose a block similarity prior model (BS-PM), which infers the coefficient distribution of an image transform-block utilizing the coefficients of similar blocks in a nonlocal area of the image. This is mainly based on the assumption that the coefficients in similar blocks usually have similar statistical properties. The quantization noise prior model (Q-PM) is also used in this paper, which employs the quantization version of coefficients as an estimation of the original ones. Based on the two models, the optimization problem in (6) is rewritten as,

$$\hat{\mathbf{x}} = \underset{\mathbf{x}}{\operatorname{argmax}}\ \mathbf{logPr}\left(\{\mathbf{Y}_{\mathcal{B}}\}_{\mathcal{B}\in\Omega_{\mathrm{CB}}}\middle|\mathbf{x}\right) + \mathbf{logPr}_{Q}(\mathbf{x}) + \mathbf{logPr}_{BS}(\mathbf{x}). \tag{7}$$

Here, $\mathrm{Pr}_{Q}(\mathbf{x})$ and $\mathrm{Pr}_{BS}(\mathbf{x})$ represent the probability distributions of Q-PM and BS-PM, respectively. These probability distributions are described in the following subsections.

A. Quantization Constraint

Since the quantization is independent for each coding block ([21]-[23]), the conditional probability for quantization value is

$$\mathbf{Pr}\left(\{\mathbf{Y}_{\mathcal{B}}\}_{\mathcal{B}\in\Omega_{\mathrm{CB}}}\middle|\mathbf{x}\right) = \prod_{\mathcal{B}\in\Omega_{\mathrm{CB}}}\mathbf{Pr}\left(\mathbf{Y}_{\mathcal{B}}|\mathbf{X}_{\mathcal{B}}\right) = \begin{cases}1, & \mathbf{Y}_{\mathcal{B}}=\mathcal{Q}(\mathbf{X}_{\mathcal{B}})\\ 0, & \mathbf{Y}_{\mathcal{B}}\neq\mathcal{Q}(\mathbf{X}_{\mathcal{B}})\end{cases}, \forall\mathcal{B}\in\Omega_{\mathrm{CB}}. \tag{8}$$

Since $\mathbf{log}(0)$ approaches negative infinity, each of the estimated coefficients in (7) should be in the quantization interval $[\mathbf{Y}_{\mathcal{B}}^{\min}(u,v),\mathbf{Y}_{\mathcal{B}}^{\max}(u,v)]$.

$$\mathbf{Y}_{\mathcal{B}}^{\min}(u,v) = \mathbf{Y}_{\mathcal{B}}(u,v) - \frac{1}{2}Q(u,v). \tag{9}$$

$$\mathbf{Y}_{\mathcal{B}}^{\max}(u,v) = \mathbf{Y}_{\mathcal{B}}(u,v) + \frac{1}{2}Q(u,v). \tag{10}$$

This requirement is referred as *quantization constraint*. It can be implemented by a projection operation, $\mathbf{X}'_{\mathcal{B}} = \mathcal{P}_{Q}(\mathbf{X}_{\mathcal{B}}, \mathbf{Y}_{\mathcal{B}})$, defined as,

$$\mathbf{X}'_{\mathcal{B}}(u,v) = \begin{cases}\mathbf{Y}_{\mathcal{B}}^{\min}(u,v), & \text{if } \mathbf{X}_{\mathcal{B}}(u,v)<\mathbf{Y}_{\mathcal{B}}^{\min}(u,v)\\ \mathbf{X}_{\mathcal{B}}(u,v), & \text{if } \mathbf{Y}_{\mathcal{B}}^{\min}(u,v)\le\mathbf{X}_{\mathcal{B}}(u,v)\le\mathbf{Y}_{\mathcal{B}}^{\max}(u,v)\\ \mathbf{Y}_{\mathcal{B}}^{\max}(u,v), & \text{if } \mathbf{X}_{\mathcal{B}}(u,v)>\mathbf{Y}_{\mathcal{B}}^{\max}(u,v)\end{cases} \tag{11}$$

B. Image Quantization Noise Prior Model

In compressed image, the noises in the coding blocks and the non-coding blocks are both caused by quantizing coding block coefficients. In this paper, we refer to them as quantization noise together. With the reconstructed coefficients in quantization intervals, the distribution of quantization noise can reflect the distribution characteristic of original coefficients in quantization intervals and is denoted as $\mathbf{Pr}_{Q}(\mathbf{x})=\mathbf{Pr}(\mathbf{X}\text{-}\mathcal{Q}(\mathbf{X}))$. There are many quantization noise models in the literatures (*e.g.* [9], [10], [24]-[26]). Robertson and Stevenson [24] utilize the Laplacian quantization noise model for quantized DCT coefficients equal to zero and uniform quantization noise model for nonzero quantized DCT coefficients. Sun and Cham [10] employed Gaussian distribution for quantization noises in the spatial domain.

In Fig. 1, we illustrate the histogram of the quantization noises for the coding blocks and the non-coding blocks in *Lena* compressed by JPEG. From Fig. 1, we can see that the quantization noises resemble Gaussian distribution in low frequency bands and resemble Laplacian distribution in high frequency bands. Therefore, we take the generalized Gaussian distribution (GGD) [38] to approximately model quantization noises with different parameters for different bands. The quantization noise distribution is formulated as follows,

$$\mathbf{Pr}_{Q}(\mathbf{x}) = \prod_{\mathcal{B}\in\Omega}\left\{\frac{v}{\beta\Gamma\left(\frac{1}{v}\right)}\exp\left\{-\left(\beta^{-1}|\mathbf{X}_{\mathcal{B}}-\mathbf{Y}_{\mathcal{B}}|\right)^{v}\right\}\right\}\cdot\delta_{Q}(\mathbf{X}_{\mathcal{B}},\mathbf{Y}_{\mathcal{B}}), \tag{12}$$

$$\delta_{Q}(\mathbf{X}_{\mathcal{B}},\mathbf{Y}_{\mathcal{B}}) = \begin{cases}1, & \mathbf{X}_{\mathcal{B}}\in\left[\mathbf{Y}_{\mathcal{B}}-\frac{1}{2}Q,\mathbf{Y}_{\mathcal{B}}+\frac{1}{2}Q\right] \text{ and } \mathcal{B}\in\Omega_{\mathrm{CB}}\\ 1, & \mathcal{B}\in\Omega_{\mathrm{NCB}}\\ 0, & \text{others}\end{cases}. \tag{13}$$

In principle, the parameter, v, in the GGD model should be estimated from a large volume of compressed image block samples. However, it is easy to observe from Fig. 1 that the quantization noise distributions in low frequency bands are close to Gaussian distribution while the quantization noise distributions in most high frequency bands can be approximated well by Laplacian distribution. Therefore, we utilize a hybrid Gaussian-Laplacian noise model in this paper. To be specific, we adopt the Gaussian model for the quantization noises in the first N_b bands and use the Laplacian model for the quantization noises in the remaining high frequency bands based on the Zig-Zag order.

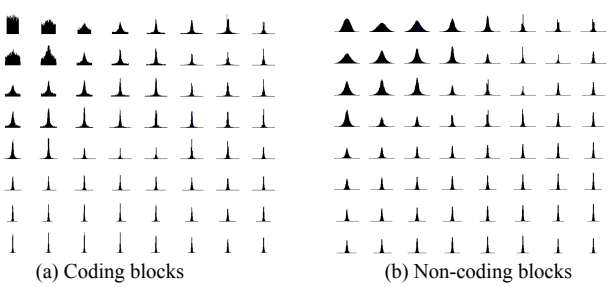

(a) Coding blocks (b) Non-coding blocks

Fig. 1: The histogram of quantization noises in the coding blocks (a) and the non-coding blocks (b) for *Lena* compressed by JPEG at quality factor 15.

C. Image Block Similarity Prior Model

Since the above Q-PM is a global prior model for natural images, it cannot reflect the variation of image local structure efficiently. Choy *et al*. [14] proposed a local smoothness prior model using the average of local coefficients as the expectation of original coefficient distribution. The prior distribution of original coefficient in [14] can be formulated as,

$$\mathbf{Pr}_{LS}(\mathbf{x})=\prod_{\mathcal{B}\in\Omega}\left\{\frac{1}{\left|\mathbf{C}_{\mathcal{N}(\mathcal{B})}\right|^{1/2}}\exp\left\{-\frac{1}{2}\left(\mathbf{X}_{\mathcal{B}}-\bar{\mathbf{X}}_{\mathcal{B}}\right)^{T}\mathbf{C}_{\mathcal{N}(\mathcal{B})}^{-1}\left(\mathbf{X}_{\mathcal{B}}-\bar{\mathbf{X}}_{\mathcal{B}}\right)\right\}\right\}, \quad (14)$$

$$\bar{\mathbf{X}}_{\mathcal{B}}=\frac{1}{\left|\mathcal{N}(\mathcal{B})\right|}\sum_{\mathcal{B}'\in\mathcal{N}(\mathcal{B})}\mathbf{X}_{\mathcal{B}'}, \quad (15)$$

$$\mathcal{N}(\mathcal{B}_{m,n})=\left\{\mathcal{B}_{k,l}\,\middle|\,m-L\le k\le m+L, n-L\le l\le n+L\right\}\setminus\left\{\mathcal{B}_{m,n}\right\}. \quad (16)$$

Here, $\mathcal{N}(\mathcal{B}_{m,n})$ is the neighborhood of block $\mathcal{B}_{m,n}$ with radius L. $|\mathcal{N}(\mathcal{B})|$ is the number of blocks in this neighborhood. $\mathbf{C}_{\mathcal{N}(\mathcal{B})}$is a diagonal matrix with the variance of neighboring coefficients, $\sigma^2_{\mathcal{N}(\mathcal{B})}(u,v)$, as its diagonal element, which is calculated by,

$$\sigma^2_{\mathcal{N}(\mathcal{B})}(u,v)=\frac{1}{\left|\mathcal{N}(\mathcal{B})\right|}\sum_{\mathcal{B}'\in\mathcal{N}(\mathcal{B})}\left(\mathbf{X}_{\mathcal{B}'}(u,v)-\bar{\mathbf{X}}_{\mathcal{B}}(u,v)\right)^2. \quad (17)$$

Unfortunately, this assumption is not reasonable for some regions, *e.g.* edges or textures.

To better infer the coefficient distribution, we propose to employ the transform-blocks with different weights as extra samples to form a prior distribution of original coefficients. In fact, it utilizes the weighted average of the coefficients in non-local blocks as the expectation of the original coefficient distribution. Here, we define the estimated transform-block as *target block*, and the ones used to infer the distribution of coefficients in the *target block* as *sample blocks*. The weight reflecting the block similarity between *sample block* and *target block*, is called *sample weight*. Based on the central limit theorem (CLT) [27], the proposed block similarity prior model is formulated as,

$$\mathbf{Pr}_{BS}(\mathbf{x})=\prod_{\mathcal{B}\in\Omega}\left\{\frac{1}{\left|\mathbf{C}_{\mathcal{N}(\mathcal{B})}\right|^{1/2}}\exp\left\{-\frac{1}{2}\left(\mathbf{X}_{\mathcal{B}}-\bar{\mathbf{X}}_{\mathcal{B}}\right)^{T}\mathbf{C}_{\mathcal{N}(\mathcal{B})}^{-1}\left(\mathbf{X}_{\mathcal{B}}-\bar{\mathbf{X}}_{\mathcal{B}}\right)\right\}\right\}, \quad (18)$$

$$\bar{\mathbf{X}}_{\mathcal{B}}=\sum_{\mathcal{B}'\in\mathcal{N}(\mathcal{B})}w_{\mathcal{B}'}\mathbf{X}_{\mathcal{B}'}, \quad (19)$$

$$\sigma^2_{\mathcal{N}(\mathcal{B})}(u,v)=\sum_{\mathcal{B}'\in\mathcal{N}(\mathcal{B})}w_{\mathcal{B}'}\left(\mathbf{X}_{\mathcal{B}}(u,v)-\bar{\mathbf{X}}_{\mathcal{B}'}(u,v)\right)^2. \quad (20)$$

Here, $w_{\mathcal{B}'}$ is the *sample weight* for block $\mathcal{B}'$ and the variance of coefficients in *sample blocks*, $\sigma^2_{\mathcal{N}(\mathcal{B})}(u,v)$, is calculated from equation (20). Based on the assumption that the similar blocks have similar statistical characteristics for transform coefficients, the more similar blocks can provide better prediction for the distribution of coefficients in *target blocks*. Therefore, higher weights should be assigned to the *sample blocks* that are more similar with the *target block*. On the other hand, lower weights should be assigned to *sample blocks* that are less similar with the *target block*, because the dissimilar *sample blocks* usually provide less meaningful information for the distribution.

In order to find reasonable *sample weights*, the relationship of block similarity and prediction accuracy needs to be investigated. Motivated by the well-known nonlocal means filter ([4], [5]), we employ the square root of difference of transform-blocks (*i.e.* L_2 norm distance in DCT domain) to measure their similarity. When the L_2 norm distance of two transform-blocks is smaller, the two blocks are more similar, vice versa. In addition, we utilize the mean square of prediction errors to measure the prediction accuracy for *target block*. In Fig. 2, the relationship between the mean square of prediction errors and block similarity is illustrated based on the uncompressed images. The horizontal axis represents the L_2 norm distance between *sample blocks* and *target blocks* in DCT domain. The vertical axis represents the mean square of prediction errors. From Fig. 2, we can see that the mean square of prediction errors increases rapidly along with the increase of the distance between *sample blocks* and *target blocks*, and their relationship can be fitted with an exponent function very well. Therefore, the *sample weights* for blocks in neighborhood $\mathcal{N}(\mathcal{B})$ are defined,

$$w_{\mathcal{B}'}=\frac{1}{Z}\exp\left\{-\frac{\left\|\mathbf{X}_{\mathcal{B}'}-\mathbf{X}_{\mathcal{B}}\right\|_2}{h}\right\}, \quad (21)$$

$$Z=\sum_{\mathcal{B}'\in\mathcal{N}(\mathcal{B})}\exp\left\{-\frac{\left\|\mathbf{X}_{\mathcal{B}'}-\mathbf{X}_{\mathcal{B}}\right\|_2}{h}\right\}. \quad (22)$$

Here, Z is the normalization constant. The parameter, h, is a smoothness factor to control the distribution of *sample weights*.

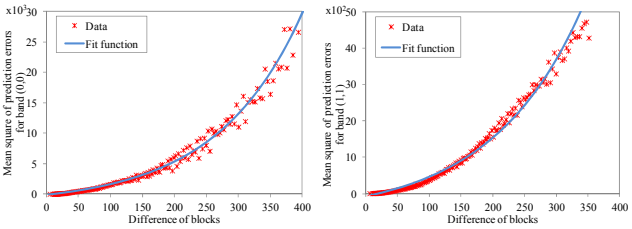

Fig. 2: The relationship of the mean square of prediction errors and the L_2 norm distance between blocks in DCT domain (over 30,000,000 blocks) fitted with exponent function.

In order to analyze the efficiency of our proposed block similarity image prior model, we compare its prediction performance with the other two image prior models. One is the local image prior model in [14] utilizing the average of local coefficients as the expectation of the original coefficients. The other one is a global image prior model that assumes the DCT transform coefficients following zero-mean Laplacian distribution, which takes zero as the expectation of original coefficients. We take some common test images, *i.e. Barbara*, *Elaine*, *Motor*, *Lena*, and *Peppers*, to calculate mean square error (MSE) of the predictions using different prior models for all the bands in 8×8 transform-blocks. Fig. 3 illustrates the MSE comparison results with the three models. We can see that the local average prior model and our proposed BS-PM achieve better prediction performance in low frequency bands than that of the Laplacian prior model, which cannot adapt to image local variants. The proposed BS-PM also has better prediction

performance than that of the local average model due to the block similarity also varying in local areas. In addition, along with the increase of the neighborhood size, more and more *sample blocks* with different structures are employed in prediction. However, they have little positive effects or even have negative effects in predicting original coefficients. They degrade the prediction performance of local average model. In the proposed BS-PM, the *sample blocks* are employed distinctively based on block similarity and the negative effects of dissimilar *sample blocks* are depressed by assigning small weights. Therefore, the BS-PM achieves the best prediction results in the three models, and the neighborhood size has little effects on its performance as illustrated in Fig. 3.

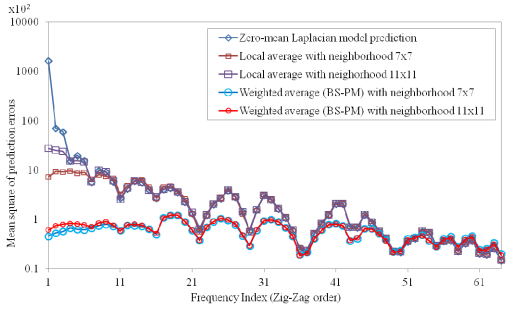

Fig. 3: The mean square error of the prediction for different image prior models on uncompressed images.

D. Block Similarity Prior Model with Compressed Images

Although the block similarity prior model has been proposed, there are still some problems when applying them to the compression artifact reduction application, where only compressed images exist. There are two variations compared with that in original images. First, we employ the reconstructed coefficients in similar transform-blocks to predict the original coefficients, but the accuracy of block similarity measurement is impaired by the presence of compression noises. Therefore, the coefficients only in low frequency bands are used to calculate the block similarity, which are not sensitive to noises. Second, we take advantage of the reconstructed values to distinguish coefficients used in prediction. Since the original coefficients lie in the quantization interval indicated by the reconstructed values, some outlier coefficients in *sample blocks*, which are far away from the reconstructed values, should be excluded to improve the prediction accuracy. Based on the two discussions, the *sample weight* for each band is rewritten as,

$$\mathbf{w}_{\mathbf{B}'}(u,v)=\frac{1}{Z}\exp\left\{-\frac{\left\|\mathbf{Y}_{\mathbf{B}'}^{M}-\mathbf{Y}_{\mathbf{B}}^{M}\right\|_2}{h}\right\}\cdot\delta_{\gamma Q}\left(\mathbf{Y}_{\mathbf{B}'}(u,v),\mathbf{Y}_{\mathbf{B}}(u,v)\right). \qquad (23)$$

Here, the step function $\delta_{\gamma Q}(\cdot)$ is utilized to exclude outliers, and γ is a constant. $\mathbf{Y}_{\mathbf{B}}^{M}$ is a vector composed of M low frequency coefficients in the left top of the transform-blocks to depress the negative effects of compression noises in block similarity measurement.

To analyze of the proposed BS-PM on compressed images, the similar experiments are carried out on images compressed by JPEG coder at different compression quality factors. Here, the quality factor (QF) is a parameter indicating the quality of compressed images, which is in the range of [0,100]. The smaller quality factors are corresponding to larger quantization steps and higher compression ratio. The relationship of the block distance in DCT domain and the mean square of prediction errors are illustrated in Fig. 4. The exponent function also can fit their relationship well at different quality factors.

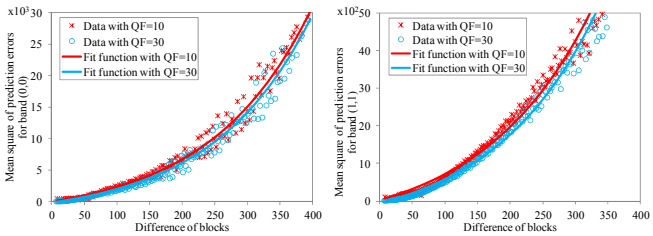

Fig. 4: The relationship of the mean square of the prediction errors and the L_2 norm distance between blocks (over 30,000,000 blocks) in compressed images at different quality factors.

In Fig. 5, we compare the prediction performance of the BS-PM and local average model on the same test images in III-C, which are compressed by JPEG at QF = 20. The *sample weight* used in Fig. 5 is calculated from equation (23). From Fig.5, we can see that the prediction performance of the proposed BS-PM is still much better than that of local average model on compressed images and is more robust to the neighborhood size due to employing block similarity and the outlier exclusion with the step function in (23). In addition, we also test the performance of BS-PM at different QFs illustrated in Fig. 6. It shows another advantage of the proposed model that the MSE of the prediction decreases along with the increase of QF. This is mainly because more and more coefficients in similar blocks are regarded as outliers and excluded along with the decrease of the quantization step.

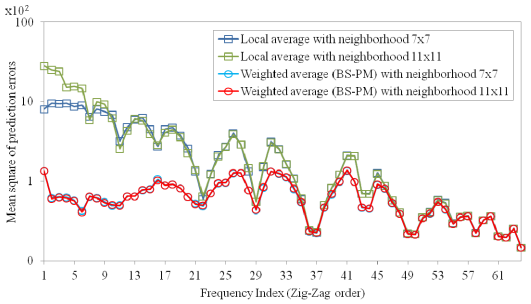

Fig. 5: The mean square error of the prediction for local average model and weighted average prediction (BS-PM) on JPEG compressed images at QF=20.

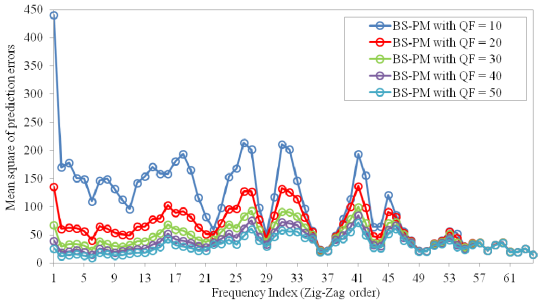

Fig. 6: The mean square error of the prediction for the weighted average prediction (BS-PM) on JPEG compressed images at different quality factors.

IV. Optimization Solution

A. Separation of Optimization Function

Under overlapped framework, the number of blocks involved in (7) equals to the total number of blocks in the image $\mathcal{I}$ and these blocks are dependent. Therefore, to make the optimization feasible, we divide the block set Ω into several subsets:

$$\Omega^{sub}(i,j)=\left\{\mathcal{B}_{m,n}\middle| m\equiv i; n\equiv j \pmod N\right\}. \quad (24)$$

Obviously, there are a total of $N\times N$ subsets (by setting i, j = 0, 1, …, N-1). Each subset forms a complete coverage of the image $\mathcal{I}$ with non-overlapped blocks except at image boundaries. To find the solution to the problem (7), we perform $N\times N$ sub-optimizations which minimizes (7) w.r.t. the variable $\mathbf{X}_{\mathcal{B}}$ in a block subset $\Omega^{sub}(i,j)$ while keeping the estimated $\mathbf{X}_{\mathcal{B}}$ in other subsets temporarily constant and irrelevant. Since the blocks in each subset are non-overlapped, the optimization problem (7) can be solved by optimizing $\mathbf{X}_{\mathcal{B}}$ in each subset separately. Assuming prior distributions being independent for different bands, the optimization solution to subset $\Omega^{sub}(i,j)$ for each band can be derived by setting the deviation of (7) to zero. The final solution is illustrated in (25)-(28). The solution (25) is used for estimating the coefficients in bands with Gaussian quantization noise distribution, and the solution (26) is used for estimating the coefficients in bands with Laplacian quantization noise distribution. From equations (25) and (26), we can see that the estimation of original coefficients is generated by adaptively fusing two prediction values based on their reliability.

$$\mathbf{X}'_{\mathcal{B}}(u,v)=\frac{\sigma^2_{\mathcal{N}(\mathcal{B})}(u,v)\mathbf{Y}_{\mathcal{B}}(u,v)}{\sigma^2_{Q}(u,v)+\sigma^2_{\mathcal{N}(\mathcal{B})}(u,v)}+\frac{\sigma^2_{Q}(u,v)\bar{\mathbf{Y}}_{\mathcal{N}(\mathcal{B})}(u,v)}{\sigma^2_{Q}(u,v)+\sigma^2_{\mathcal{N}(\mathcal{B})}(u,v)},\ \mathcal{B}\in\Omega^{sub}(i,j). \quad (25)$$

$$\mathbf{X}'_{\mathcal{B}}(u,v)=\begin{cases}\bar{\mathbf{Y}}_{\mathcal{N}(\mathcal{B})}(u,v)-\dfrac{\sqrt{2}\sigma^2_{\mathcal{N}(\mathcal{B})}(u,v)}{\sigma_{Q}(u,v)} & \bar{\mathbf{Y}}_{\mathcal{N}(\mathcal{B})}(u,v)-\mathbf{Y}_{\mathcal{B}}(u,v)>\dfrac{\sqrt{2}\sigma^2_{\mathcal{N}(\mathcal{B})}(u,v)}{\sigma_{Q}(u,v)}\\ \mathbf{Y}_{\mathcal{B}}(u,v) & -\dfrac{\sqrt{2}\sigma^2_{\mathcal{N}(\mathcal{B})}(u,v)}{\sigma_{Q}(u,v)}\le\bar{\mathbf{Y}}_{\mathcal{N}(\mathcal{B})}(u,v)-\mathbf{Y}_{\mathcal{B}}(u,v)\le\dfrac{\sqrt{2}\sigma^2_{\mathcal{N}(\mathcal{B})}(u,v)}{\sigma_{Q}(u,v)}\\ \bar{\mathbf{Y}}_{\mathcal{N}(\mathcal{B})}(u,v)+\dfrac{\sqrt{2}\sigma^2_{\mathcal{N}(\mathcal{B})}(u,v)}{\sigma_{Q}(u,v)} & \bar{\mathbf{Y}}_{\mathcal{N}(\mathcal{B})}(u,v)-\mathbf{Y}_{\mathcal{B}}(u,v)<-\dfrac{\sqrt{2}\sigma^2_{\mathcal{N}(\mathcal{B})}(u,v)}{\sigma_{Q}(u,v)}\end{cases} \quad (26)$$

$$\bar{\mathbf{Y}}_{\mathcal{N}(\mathcal{B})}(u,v)=\sum_{\mathcal{B}'\in\Omega^{sub}(i,j),\ \mathcal{B}\in\Omega^{sub}(i,j)}\mathbf{w}_{\mathcal{B}'}(u,v)\mathbf{Y}_{\mathcal{B}'}(u,v) \quad (27)$$

$$\hat{\mathbf{X}}_{\mathcal{B}}=\mathcal{P}_{Q}(\mathbf{X}'_{\mathcal{B}},\mathbf{Y}_{\mathcal{B}})\quad \mathcal{B}\in\Omega_{\mathrm{CB}}. \quad (28)$$

B. Enforcement of Quantization Constraint

According to (25)-(28), the optimization in (7) for each subset can be easily solved. However, the quantization constraint in (28) is limited to the sub-optimization solution of $\Omega^{sub}(0,0)$. When i and j are not zero simultaneously, the blocks in $\Omega^{sub}(i,j)$ correspond to non-coding blocks. In this case, to enforce the quantization constraint, the optimization solution to each subset can be obtained as follows: (1) for every block in $\Omega^{sub}(i,j)$, find the optimal estimation $\mathbf{X}'_{\mathcal{B}}$ via equation (25) and (26); (2) construct the whole estimated image by inversely transforming all the estimated blocks in this subset; (3) divide the estimated image into blocks as $\Omega^{sub}(0,0)$ and convert them to block-DCT domain; (4) apply the quantization constraint operation in (28) to blocks generated in stage (3); (5) convert estimated blocks in stage (4) to the spatial domain, and get the estimated image for the subset.

C. Adaptive Parameter Selection and Algorithm Description

In image process algorithms, different parameter sets may affect the performance of algorithms significantly. For practical algorithms, the parameters should be constant or decided adaptively. In our proposed scheme, there are six parameters to be decided, *i.e.*, the first N_b bands with Gaussian quantization noise distribution, the parameter M and γ in (23) used in *sample weight*, the variance of the quantization noises σ^2_Q, the neighborhood size L, and the smoothness factor h in (23). We set N_b as 10 for all the experiments empirically. For the parameters M and γ, we simply set them as 16 and 6 for 8×8 blocks respectively, which do not have significantly influence on the performance. For the variance of quantization noises, we estimate it from the quantization step in this paper,

$$\sigma^2_Q(u,v)=\frac{1}{\alpha}Q^2(u,v). \quad (29)$$

For JPEG compressed images, we set α set as 7 and 0.5 for Gaussian quantization noise and Laplacian quantization noise respectively.

For the parameters, L and h, which have obvious influence on the final performance, we employ some test images to find the reasonable parameter values. The test images, *Airplane*, *Barbara*, *Motor*, *Elaine*, *Lena* and *Peppers*, are compressed by JPEG at different QFs. Firstly, we test the effect of the neighborhood size according to objective quality of estimated images measured by peak signal-noise ratio (PSNR). In Fig. 7, we illustrate the results of *Lena* with size of 256×256 and *Airplane* with size of 384×256, for different neighborhood sizes and QFs with the same smoothness factor h. It can be easily observed that the performance of our proposed scheme is improved along with the increase of the neighborhood size, L, at different QFs. When L is beyond 8, the performance is almost stable. Considering the performance and complexity, we take the parameter L as 8 in our scheme.

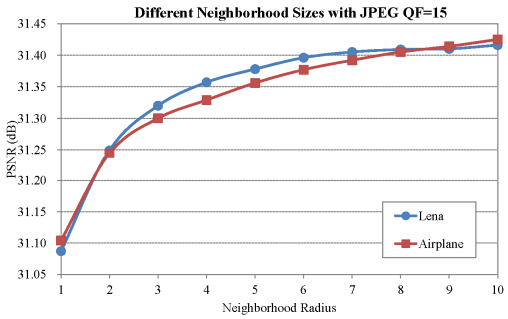

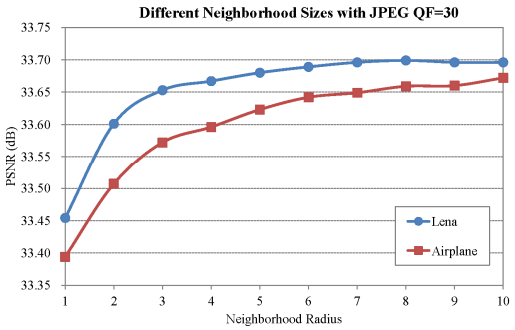

Fig. 7: The performance of our proposed method with different neighborhood sizes.

Secondly, we search for the best smoothness factor, h, given the neighborhood size parameter as 8. Based on the previous research, *e.g.* nonlocal means filter [4] [5], the smoothness factor is closely related to compression noise levels. For simplicity, in this paper, we take quantization step of DC band, $Q(0,0)$, as a measurement of compression noise levels, which can be obtained from the compressed bitstream. In order to find the relationship between h and $Q(0,0)$, we try out h from 5 to 60 with increment one for the test images, *Barbara*, *Elaine*, *Lena*, *Pepper* with size 512×512 and *Motor* with size 768×512, compressed by JPEG at QFs in {5, 10, 15, 20 … 90}. The relationship between h and QF is approximately expressed by linear regression in Eqn. (30).

$$h = \begin{cases} 0.2546Q(0,0) + 12.557 & Q(0,0) \geq 16 \\ 16.63 & Q(0,0) < 16 \end{cases} \quad (30)$$

Based on the above discussion, our proposed algorithm is described as follows.

Our Proposed Algorithm for compression artifact reduction

Input: Compressed image: **Y**;

Output: Denoised image: $\hat{\mathbf{x}}$;

1: Parameter Initialization: L, h, M, α;

2: **if** subset is $\Omega^{sub}(0,0)$ do

3: Estimate all the transform blocks in current subset via (25) and (26);

4: Apply quantization constraint to all the estimated blocks via (28);

5: Transform all the blocks obtained in step 4 into the spatial domain to generate the estimated image $\mathbf{z}(0,0)$;

6: **end**

7: **For** each subset $\Omega^{sub}(i,j)$ $(i+j \neq 0)$ do

8: Estimate all the transform blocks in current subset via (25) and (26);

9: Transform all the estimated blocks into the spatial domain to generate the estimated image $\mathbf{z}'(i,j)$;

10: Divide the estimated image into non-overlapped blocks as the ones in $\Omega^{sub}(0,0)$, and apply quantization constraint to these blocks via (28);

11: Transform all the blocks obtained in step 10 into the spatial domain to generate the estimated image $\mathbf{z}(i,j)$;

12: **end**

13: Combine all the estimated images $\mathbf{z}(i,j)$ to generate the output image $\hat{\mathbf{x}}$.

V. Experiment Results

In this section, we first test the performance of the overlapped strategy. The overlapped step size is defined as the distance between two adjacent blocks to be estimated. If the overlapped step size is the same as the block size, all the blocks are non-overlapped. If the overlapped step size is 1, there is only one column of pixels are different between the two adjacent blocks in horizontal direction. In Fig. 8, the performance of different overlapped step sizes for images, *Lean*, *Peppers* with size of 512×512 and *Parrot* with size of 768×512 compressed by JPEG at QF=15 is tested. The results illustrate that the smaller overlapped step size provides the higher quality of restored images. This is mainly because more predictions are generated for the image with smaller overlapped step sizes. In addition, the overlapped strategy takes advantage of the correlations between blocks to depress the blocking artifacts.

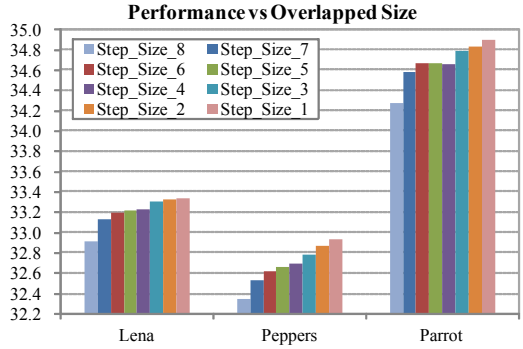

Fig. 8: The performance of our proposed method with different overlapped step sizes. The images are compressed by JPEG at QF=15.

We also evaluate the performance of the proposed method with state-of-the-art compression artifact reduction algorithms and denoising algorithms, including Choy's method [14], the nonlocal means filter (NLM) [5], BM3D method [28], PSW [29], Nosratinia's method [30], steering kernel regression (SKR) [6], KSVD [31], Sun's method [10] and PLOW [32]. The test images in our experiments includes popular images *Barbara*, *Fishingboat*, *Lena*, *Peppers* with size of 512×512, *Cameraman* with size of 256×256 and Kodak image set, as listed in Table I. These gray images are first encoded by a JPEG coder [33] with different quality factors and then reconstructed using standard JPEG decoder and different compression artifact reduction methods. For our proposed method, the parameter L is set as 8 and the smoothness factor h is set according to (30). For the compared methods, we also try out many parameters with some test images to find the reasonable ones under different compression ratios. Table I illustrates the PSNR results of the reconstructed images with different methods. Our proposed scheme outperforms all of the other methods and achieves up to 1.19dB gain over JPEG decoder on average. Compared with other artifact reduction methods, our proposed method also achieves about 0.25~0.75dB on average. Especially, our method achieves up to 1.50dB gains over JPEG for image *Parrot*. In table II, we illustrate the Structural Similarity Index Metric (SSIM) results of the reconstructed images. The SSIM is another image quality assessment method, which is known to be able to provide a more consistent measurement of image quality with human eye perception [36].

Our proposed method also achieves better performance compared with other methods on average. The best results are highlighted for each image in Table I and Table II. Fig. 9 shows the reconstruction quality and the improvement vary with JPEG quality factors. We can see that our proposed scheme works well over a wide quality (or bit rate) range. Especially, for the image *Barbara*, the performance of our proposed method is much better than that of others due to lots of similar patches existing in this image.

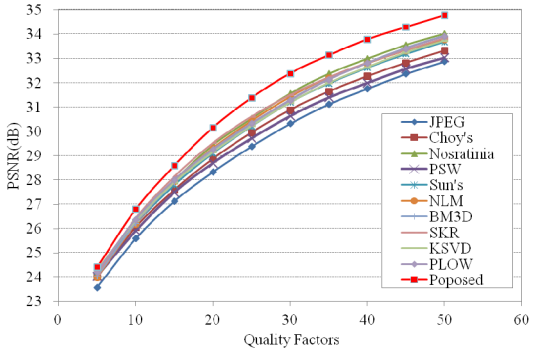

(a) Barbara

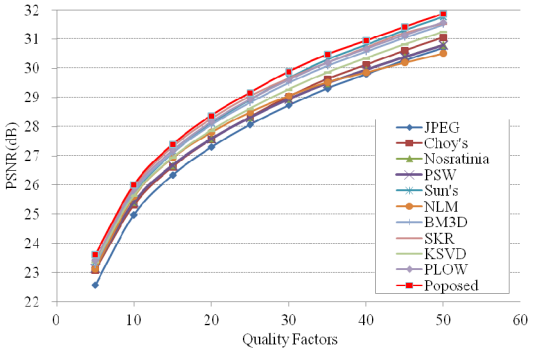

(b) Motor

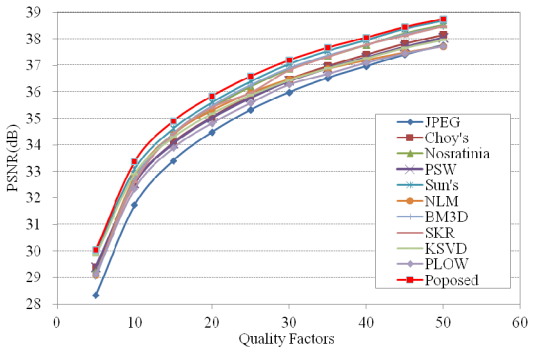

(c) Parrot

Fig. 9: The quality of the reconstructed images with different methods at different compression quality factors.

To evaluate the influence of noise models, we compare the performance of two alternative quantization noise models with the hybrid Gaussian-Laplacian noise model used in our proposed method. The other two quantization noise modeling schemes use the Gaussian distribution alone and the Laplacian distribution alone, respectively. We denote the compression artifact reduction method with Gaussian quantization noise model alone as Method-G and the other method with Laplacian quantization noise model alone as Method-L. Table III illustrates PSNR results of the three methods. We can see that the three methods achieve very similar performance (with difference smaller than 0.2dB and average difference smaller than 0.02dB), which suggests that the three quantization noise models do not have significant difference on the overall performance. The reason is that in our framework, we estimate the original coefficients by adaptively fusing the two predictions, *i.e.*, predicted coefficients from the decoded image and from the group of similar blocks. The weights of the two predictions are determined by their variance. Since coefficients from the group of similar blocks with current block fall into a small range constrained by quantization intervals, their variance in general is much smaller than that of coefficient quantization errors in current block, which is formed by all possible image blocks. Therefore, the prediction from the group of similar bocks will dominate the ultimate prediction result.

In Fig. 10, we illustrate the mean square error of coefficients for *Lena*, reconstructed with our proposed method and JPEG for different bands. We can see that our proposed method can significantly reduce the mean square error of coefficients in low and middle frequency bands.

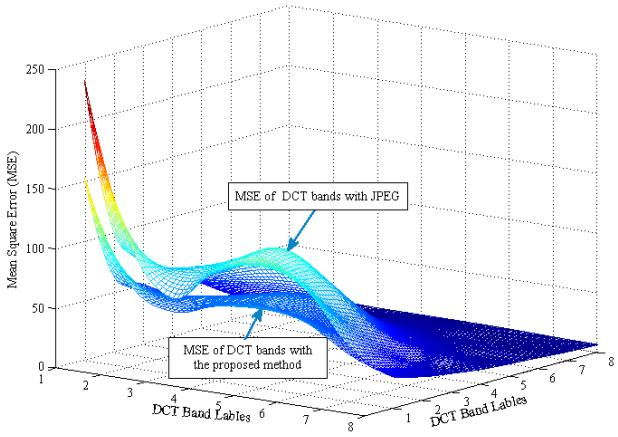

Fig. 10: The mean square error of coefficients in coding blocks for *Lena* reconstructed by the proposed method and JPEG.

In Fig. 11 and 12, we show the subjective quality of the reconstructed images which are also compressed at QF=15. From the subjective quality comparison, we can see that the compression artifacts are obvious in the images reconstructed by the standard JPEG decoder. The compared methods are able to reduce the compression artifacts partially, but some blocking and ringing artifacts are still observed obviously in the images, *e.g.* on the airscrew in Fig. 11 and on the back of the rider in Fig.12. Our proposed method produces more pleasing visual quality than that of other methods, especially in the region of the red box. It does not only reduce most of the compression artifacts significantly, but also preserves image edges very well.

In the following experiment, we compare our proposed method with the in-loop filter of H.264/AVC [35]. The software of H.264/AVC is JM18.2 [36]. The sequences are common test sequences with WQVGA format widely used in

video coding standards, *BaskeballPass*, *BQSquare*, *BlowingBubbles*, *RaceHorses*. These sequences are compressed with intra coding method of H.264/AVC, in which we make only 8×8 block partition enable for convenience. The quantization parameters are set as 37 and 47 respectively. The parameter α in (29) is set as 25 for Gaussian quantization noise distribution and 20 for Laplacian quantization noise distribution, because the transform coefficients of the prediction residuals are more concentrated around zero, which causes the quantization noises with a lower variance. The other parameters are the same as the above experiments. Table IV and V illustrate the objective quality of the luminance component with two quality assessment methods, PSNR and SSIM. Our proposed method achieves up to 0.31 dB gain over the in-loop filter of H.264/AVC for *RaceHorses* at QP=37. On average, our proposed method achieves 0.20 dB gain over in-loop filter of H.264/AVC at QP=37, and achieves 0.16 dB gain at QP=47.

VI. Conclusion

In this paper, we propose a new transform-domain approach to reduce the compression artifacts. In the proposed scheme, the transform coefficients of a compressed image are restored by adaptive estimation of DCT coefficients in overlapped transform-blocks. The quality of restored images is improved via combining the quantization noise model and block similarity prior model. To tackle the optimization problem, the overlapped blocks are divided into several subsets containing non-overlapped blocks so that the overall optimization is reduced to a set of sub-optimization problems that can be easily solved. An effective parameter selection method is proposed to make our scheme more practical. Experimental results demonstrate that our proposed method can remarkably improve both the subjective and the objective quality of the block transform coded images.

TABLE I: PSNR results of restored images using different methods for test images compressed by JPEG at QF = 15 (Unit: dB).

TestImages	JPEG	Choy's	Nosratinia's	PSW	Sun's	NLM	BM3D	SKR	KSVD	PLOW	Proposed
Barbara	27.14	27.59	27.97	27.49	27.80	27.95	27.90	28.15	27.91	28.01	**28.60**
Cameraman	27.71	27.84	28.24	27.93	28.45	28.14	28.33	28.38	28.26	28.37	**28.67**
FishingBoat	29.53	29.93	30.28	29.94	30.43	30.19	30.41	30.41	30.22	30.44	**30.57**
Lena	31.94	32.63	32.93	32.71	33.10	32.95	33.11	33.12	32.95	33.22	**33.34**
Peppers	31.54	32.16	32.43	32.20	32.78	32.43	32.59	32.57	32.58	32.65	**32.94**
Hats	32.09	32.58	32.80	32.59	33.07	33.04	33.07	32.76	33.03	32.74	**33.32**
Kodim04	31.22	31.70	31.86	31.65	32.03	31.92	32.07	31.84	31.81	31.77	**32.15**
Motor	26.34	26.63	26.95	26.67	27.10	26.93	27.10	27.31	26.94	27.20	**27.39**
Window	31.36	31.91	32.29	31.89	32.56	32.43	32.58	32.25	32.39	32.26	**32.74**
Sailboats	31.58	32.00	32.37	31.96	32.62	32.37	32.47	31.65	32.45	32.19	**32.75**
Sailboats2	31.20	31.56	31.96	31.54	32.15	32.05	32.21	31.84	31.93	31.89	**32.46**
Statue	30.52	30.94	31.21	30.96	31.35	31.19	31.38	31.29	31.14	31.09	**31.48**
Tower	29.13	29.44	29.81	29.56	29.92	29.73	29.90	29.81	29.72	29.89	**30.19**
Airplane	30.92	31.15	31.41	31.22	31.71	31.50	31.67	31.41	31.50	31.29	**31.91**
Parrot	33.40	34.09	34.38	34.06	34.61	34.41	34.42	34.39	34.29	33.88	**34.90**
Average	30.37	30.81	31.13	30.83	31.31	31.15	31.28	31.15	31.14	31.12	**31.56**

TABLE II: SSIM results of restored images using different methods for test images compressed by JPEG at QF = 15 .

TestImages	JPEG	Choy's	Nosratinia's	PSW	Sun's	NLM	BM3D	SKR	KSVD	PLOW	Proposed
Barbara	0.816	0.824	0.830	0.830	0.832	0.841	**0.845**	0.833	0.838	0.843	0.844
Cameraman	0.836	0.845	0.854	0.844	**0.863**	0.858	0.858	0.852	0.850	0.858	0.862
FishingBoat	0.804	0.815	0.825	0.813	0.823	0.823	**0.828**	0.824	0.807	0.826	0.827
Lena	0.852	0.872	0.876	0.873	0.878	0.878	0.879	0.877	0.870	0.881	**0.882**
Peppers	0.817	0.838	0.843	0.839	0.849	0.845	0.845	0.845	0.842	0.847	**0.850**
Hats	0.859	0.875	0.880	0.875	0.884	0.885	0.883	0.880	0.880	0.877	**0.887**
Kodim04	0.809	0.824	0.828	0.822	0.828	0.827	**0.831**	0.826	0.815	0.824	**0.831**
Motor	0.808	0.818	0.829	0.817	0.831	0.831	**0.838**	0.835	0.822	0.836	0.836
Window	0.889	0.908	0.916	0.908	0.921	0.921	0.920	0.916	0.915	0.915	**0.923**
Sailboats	0.867	0.880	0.887	0.878	0.890	0.890	0.887	0.885	0.885	0.882	**0.893**
Sailboats2	0.846	0.860	0.869	0.858	0.871	0.873	0.875	0.869	0.861	0.870	**0.876**
Statue	0.838	0.858	0.864	0.859	0.867	0.866	0.867	0.866	0.855	0.863	**0.869**
Tower	0.811	0.820	0.825	0.819	0.824	0.823	0.826	0.821	0.811	0.822	**0.827**
Airplane	0.873	0.879	0.884	0.878	0.887	0.886	0.886	0.883	0.878	0.882	**0.888**
Parrot	0.884	0.907	0.910	0.907	0.915	0.913	0.910	0.910	0.905	0.906	**0.916**
Average	0.841	0.855	0.861	0.855	0.864	0.864	0.865	0.861	0.856	0.862	**0.867**

TABLE III: PSNR RESULTS OF RESTORED IMAGES USING DIFFERENT QUANTIZATION NOISE MODELS FOR TEST IMAGES COMPRESSED BY JPEG (Unit: dB).

TestImages	QF=15			QF=25			QF=35			QF=45		
	Method-G	Method-L	Proposed	Method-G	Method-L	Proposed	Method-G	Method-L	Proposed	Method-G	Method-L	Proposed
Barbara	28.54	28.62	28.60	31.26	31.40	31.39	33.03	33.15	33.14	34.20	34.29	34.30
Cameraman	28.69	28.66	28.67	30.27	30.23	30.22	31.49	31.44	31.42	32.39	32.30	32.28
FishingBoat	30.57	30.56	30.57	32.20	32.18	32.19	33.28	33.26	33.26	34.02	33.99	33.99
Lena	33.34	33.34	33.34	34.85	34.84	34.84	35.72	35.71	35.70	36.39	36.38	36.37
Peppers	32.94	32.94	32.94	34.12	34.12	34.12	34.79	34.79	34.78	35.30	35.29	35.29
Hats	33.31	33.31	33.32	34.91	34.92	34.92	35.98	35.97	35.98	36.85	36.83	36.84
Kodim04	32.15	32.13	32.15	33.67	33.65	33.67	34.62	34.59	34.60	35.32	35.27	35.28
Motor	27.38	27.38	27.39	29.18	29.17	29.17	30.53	30.48	30.48	31.51	31.43	31.42
Window	32.72	32.73	32.74	34.59	34.60	34.61	35.75	35.74	35.75	36.67	36.65	36.66
Sailboats	32.77	32.74	32.75	34.45	34.43	34.44	35.57	35.53	35.53	36.38	36.34	36.34
Sailboats2	32.44	32.45	32.46	34.24	34.25	34.25	35.42	35.42	35.42	36.23	36.21	36.22
Statue	31.48	31.48	31.48	33.14	33.12	33.13	34.23	34.21	34.21	35.06	35.01	35.01
Tower	30.19	30.17	30.19	31.80	31.77	31.77	32.86	32.81	32.81	33.66	33.61	33.61
Airplane	31.91	31.91	31.91	33.50	33.49	33.50	34.56	34.53	34.53	35.34	35.29	35.29
Parrot	34.90	34.88	34.90	36.60	36.58	36.59	37.70	37.67	37.67	38.49	38.45	38.44
Average	31.56	31.55	31.56	33.25	33.25	33.25	34.37	34.35	34.35	35.18	35.16	35.16

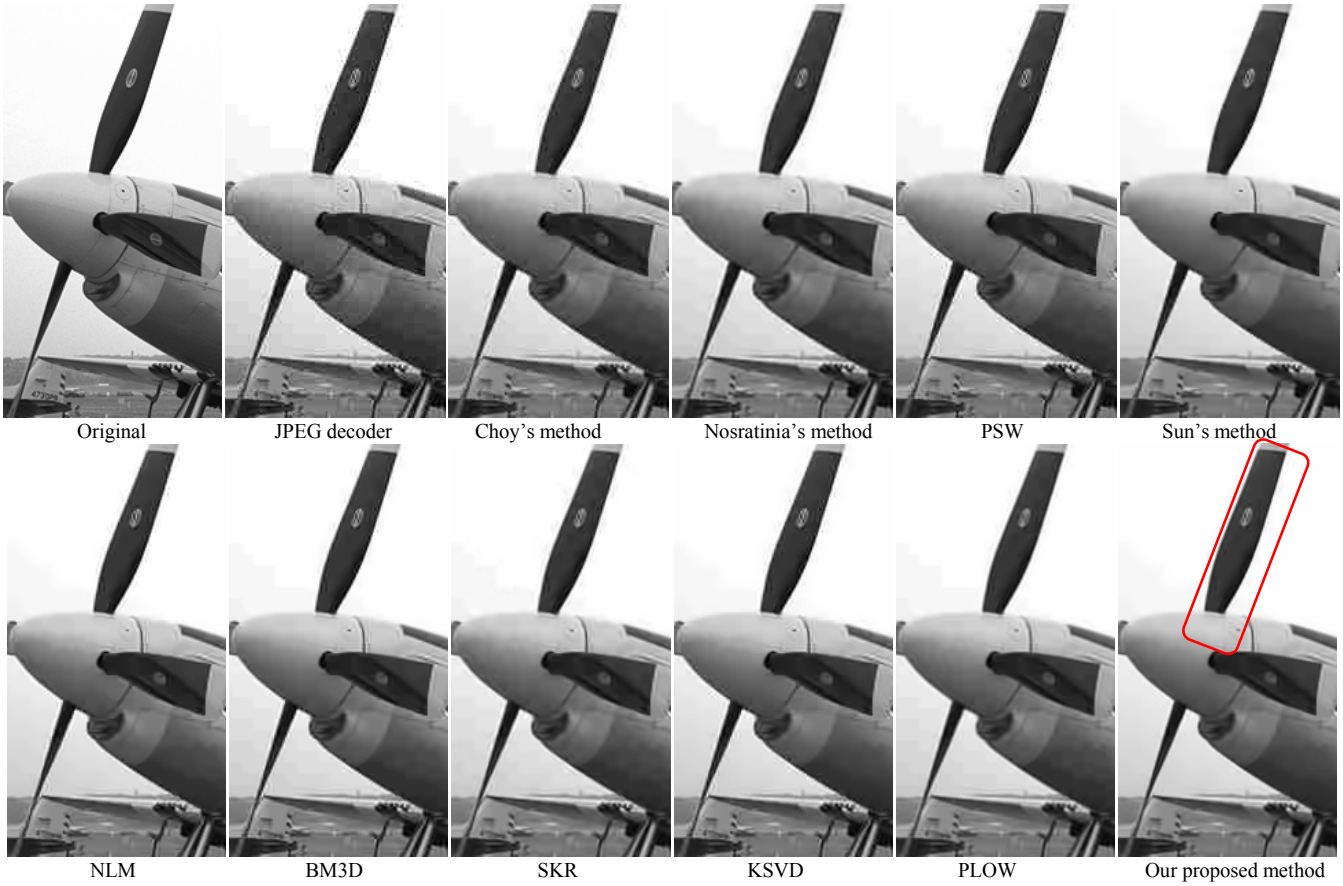

Fig. 11: The reconstructed images with different methods. The test image, *Airplane*, is compressed by JPEG at QF = 15.

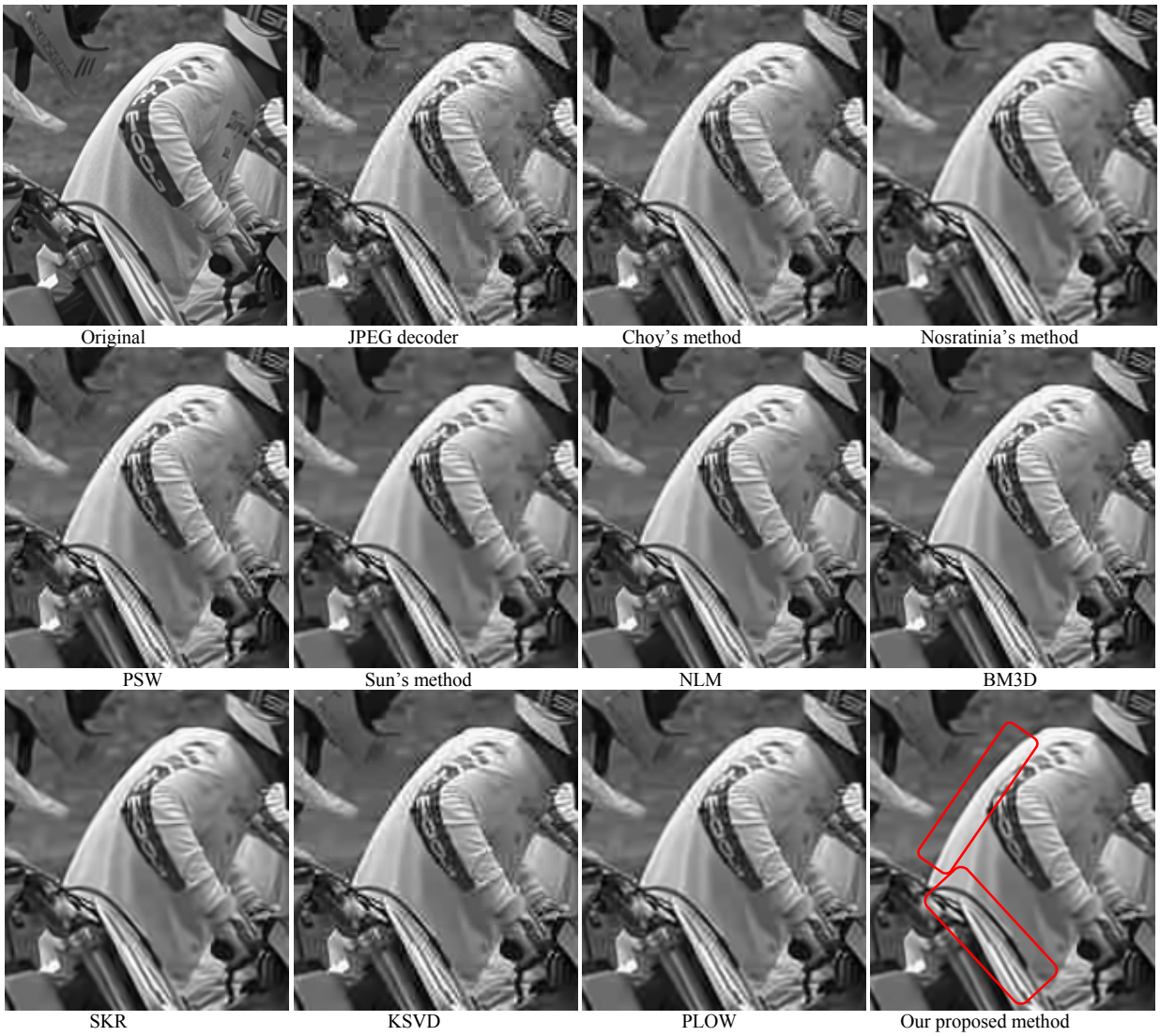

Fig.12: The reconstructed images with different methods. The test image, *Motor*, is compressed by JPEG at QF = 15.

TABLE IV
OBJECTIVE QUALITY OF RESTORED IMAGES USING DIFFERENT METHODS FOR TEST IMAGES COMPRESSED WITH H.264 INTRA CODING AND $QP = 37$.

Test Images	H.264 w/o Deblocking		H.264 Deblocking		Proposed	
	PSNR	SSIM	PSNR	SSIM	PSNR	SSIM
BQSquare	28.68	0.843	28.79	0.849	**28.88**	**0.859**
BasketballPass	31.94	0.844	32.21	0.852	**32.45**	**0.857**
BlowingBubbles	29.98	0.815	30.15	0.822	**30.34**	**0.827**
RaceHorses	30.25	0.839	30.46	0.847	**30.77**	**0.855**
Average	30.21	0.835	30.40	0.843	**30.60**	**0.850**

TABLE V
OBJECTIVE QUALITY OF RESTORED IMAGES USING DIFFERENT METHODS FOR TEST IMAGES COMPRESSED WITH H.264 INTRA CODING AND $QP = 47$.

Test Images	H.264 w/o Deblocking		H.264 Deblocking		Proposed	
	PSNR	SSIM	PSNR	SSIM	PSNR	SSIM
BQSquare	21.96	0.677	22.14	0.693	**22.35**	**0.707**
BasketballPass	26.31	0.680	26.59	0.698	**26.76**	**0.705**
BlowingBubbles	24.62	0.581	24.95	0.611	**25.03**	**0.614**
RaceHorses	24.60	0.634	24.97	0.667	**25.12**	**0.675**
Average	24.37	0.643	24.66	0.667	**24.82**	**0.675**

APPENDIX

In order to solve the sub-optimization problem, we substitute the probabilities in (8), (12) and (18) into (7). For the bands with Gaussian quantization noise distribution, the optimization problem is formulated as,

$$\begin{aligned}\hat{\mathbf{x}} &= \arg\max_{\mathbf{x}} \mathbf{log}\mathbf{Pr}_{Q}(\mathbf{x}) + \mathbf{log}\mathbf{Pr}_{BS}(\mathbf{x}) \\ &= \arg\max_{\mathbf{x}} \mathbf{log} \prod_{\mathcal{B}\in\Omega^{sub}(i,j)} \left\{ \frac{1}{|\mathbf{C}_{Q}|^{1/2}} \exp\left\{ -\frac{1}{2}\left(\mathbf{X}_{\mathcal{B}}-\mathbf{Y}_{\mathcal{B}}\right)^{T} \mathbf{C}_{Q}^{-1}\left(\mathbf{X}_{\mathcal{B}}-\mathbf{Y}_{\mathcal{B}}\right) \right\} \right\} \\ &+ \mathbf{log} \prod_{\mathcal{B}\in\Omega^{sub}(i,j)} \left\{ \frac{1}{|\mathbf{C}_{\mathcal{N}(\mathcal{B})}|^{1/2}} \exp\left\{ \frac{1}{2}\left(\mathbf{X}_{\mathcal{B}}-\bar{\mathbf{Y}}_{\mathcal{N}(\mathcal{B})}\right)^{T} \mathbf{C}_{\mathcal{N}(\mathcal{B})}^{-1}\left(\mathbf{X}_{\mathcal{B}}-\bar{\mathbf{Y}}_{\mathcal{N}(\mathcal{B})}\right) \right\} \right\}\end{aligned} \tag{31}$$

$$\mathbf{C}_{Q} = diag\left(\sigma_{Q}^{2}(0,0),\sigma_{Q}^{2}(0,1),\ldots,\sigma_{Q}^{2}(0,N-1),\sigma_{Q}^{2}(1,0),\ldots,\sigma_{Q}^{2}(N-1,N-1)\right),$$

$$\mathbf{C}_{\mathcal{N}(\mathcal{B})} = diag\left(\sigma_{\mathcal{N}(\mathcal{B})}^{2}(0,0),\sigma_{\mathcal{N}(\mathcal{B})}^{2}(0,1),\ldots,\sigma_{\mathcal{N}(\mathcal{B})}^{2}(0,N-1),\sigma_{\mathcal{N}(\mathcal{B})}^{2}(1,0),\ldots,\sigma_{\mathcal{N}(\mathcal{B})}^{2}(N-1,N-1)\right).$$

Here, $\mathbf{X}_{\mathcal{B}}$, $\mathbf{Y}_{\mathcal{N}(\mathcal{B})}$ and $\overline{\mathbf{Y}}_{\mathcal{B}}$ are vectors whose elements are taken

row-wise from corresponding blocks. The function, *diag*(·), constructs a diagonal matrix with its elements. Assuming that the blocks in image $\mathcal{I}$ are independent, the optimization problem in (31) is equal to that in (32) for all the blocks in $\Omega^{sub}(i,j)$.

$$\mathbf{X}'_{\mathcal{B}} = \underset{\mathbf{X}_{\mathcal{B}}}{\operatorname{argmin}} \frac{1}{2}\left(\mathbf{X}_{\mathcal{B}}-\mathbf{Y}_{\mathcal{B}}\right)^{T}\mathbf{C}_{Q}^{-1}\left(\mathbf{X}_{\mathcal{B}}-\mathbf{Y}_{\mathcal{B}}\right) + \frac{1}{2}\left(\mathbf{X}_{\mathcal{B}}-\bar{\mathbf{Y}}_{\mathcal{N}(\mathcal{B})}\right)^{T}\mathbf{C}_{\mathcal{N}(\mathcal{B})}^{-1}\left(\mathbf{X}_{\mathcal{B}}-\bar{\mathbf{Y}}_{\mathcal{N}(\mathcal{B})}\right) \quad (32)$$

Therefore, the solution of optimization problem in (32) is derived by setting its derivative to zero w.r.t. $\mathbf{X}_{\mathcal{B}}$ in each block subset.

$$\mathbf{C}_{Q}^{-1}\left(\mathbf{X}_{\mathcal{B}}-\mathbf{Y}_{\mathcal{B}}\right)+\mathbf{C}_{\mathcal{N}(\mathcal{B})}^{-1}\left(\mathbf{X}_{\mathcal{B}}-\bar{\mathbf{Y}}_{\mathcal{N}(\mathcal{B})}\right)=0\,. \quad (33)$$

The solution is derived as follows.

$$\mathbf{X}'_{\mathcal{B}}=\left(\mathbf{C}_{Q}^{-1}+\mathbf{C}_{\mathcal{N}(\mathcal{B})}^{-1}\right)^{-1}\left(\mathbf{C}_{Q}^{-1}\mathbf{Y}_{\mathcal{B}}+\mathbf{C}_{\mathcal{N}(\mathcal{B})}^{-1}\bar{\mathbf{Y}}_{\mathcal{N}(\mathcal{B})}\right). \quad (34)$$

Because the two matrices $\mathbf{C}_{Q}^{-1}$ and $\mathbf{C}_{\mathcal{N}(\mathcal{B})}^{-1}$ are diagonal ones, the solution for bands in (26) is obtained by substituting the matrices with their elements.

$$\mathbf{X}'_{\mathcal{B}}(u,v)=\frac{\sigma_{\mathcal{N}(\mathcal{B})}^{2}(u,v)\mathbf{Y}_{\mathcal{B}}(u,v)}{\sigma_{Q}^{2}(u,v)+\sigma_{\mathcal{N}(\mathcal{B})}^{2}(u,v)}+\frac{\sigma_{Q}^{2}(u,v)\bar{\mathbf{Y}}_{\mathcal{N}(\mathcal{B})}(u,v)}{\sigma_{Q}^{2}(u,v)+\sigma_{\mathcal{N}(\mathcal{B})}^{2}(u,v)}\,. \quad (35)$$

For the bands with Laplacian quantization noise distribution, the optimization problem is formulated as,

$$\begin{aligned}\hat{\mathbf{x}} &= \underset{\mathbf{x}}{\operatorname{argmax}}\ \mathbf{logPr}_{Q}(\mathbf{x})+\mathbf{logPr}_{BS}(\mathbf{x})\\ &= \underset{\mathbf{x}}{\operatorname{argmax}}\ \mathbf{log}\prod_{\mathcal{B}\in\Omega^{sub}(i,j)}\left\{\frac{1}{\sqrt{2}\left|\mathbf{C}_{Q}\right|^{1/2}}\exp\left\{-\sqrt{2}\mathbf{C}_{Q}^{-\frac{1}{2}}\left|\mathbf{X}_{\mathcal{B}}-\mathbf{Y}_{\mathcal{B}}\right|\right\}\right\}\\ &+\mathbf{log}\prod_{\mathcal{B}\in\Omega^{sub}(i,j)}\left\{\frac{1}{\left|\mathbf{C}_{\mathcal{N}(\mathcal{B})}\right|^{1/2}}\exp\left\{-\frac{1}{2}\left(\mathbf{X}_{\mathcal{B}}-\bar{\mathbf{Y}}_{\mathcal{N}(\mathcal{B})}\right)^{T}\mathbf{C}_{\mathcal{N}(\mathcal{B})}^{-1}\left(\mathbf{X}_{\mathcal{B}}-\bar{\mathbf{Y}}_{\mathcal{N}(\mathcal{B})}\right)\right\}\right\}\end{aligned} \quad (36)$$

The optimization process is similar with that in [37]. The derivative of the equation (36) is set to zero w.r.t. $\mathbf{X}_{\mathcal{B}}$ in each block subset.

$$\sqrt{2}\mathbf{C}_{Q}^{-\frac{1}{2}}sign\left(\mathbf{X}_{\mathcal{B}}-\mathbf{Y}_{\mathcal{B}}\right)+\mathbf{C}_{\mathcal{N}(\mathcal{B})}^{-1}\left(\mathbf{X}_{\mathcal{B}}-\bar{\mathbf{Y}}_{\mathcal{N}(\mathcal{B})}\right)=0\,, \quad (37)$$

$$sign(x)=\begin{cases}1 & x>0\\ 0 & x=0\\ -1 & x<0\end{cases}. \quad (38)$$

The solution for bands in (27) is obtained by substituting the matrices with their elements.

$$\mathbf{X}'_{\mathcal{B}}(u,v)=\begin{cases}\bar{\mathbf{Y}}_{\mathcal{N}(\mathcal{B})}(u,v)-\dfrac{\sqrt{2}\sigma_{\mathcal{N}(\mathcal{B})}^{2}(u,v)}{\sigma_{Q}(u,v)} & \bar{\mathbf{Y}}_{\mathcal{N}(\mathcal{B})}(u,v)-\mathbf{Y}_{\mathcal{B}}(u,v)>\dfrac{\sqrt{2}\sigma_{\mathcal{N}(\mathcal{B})}^{2}(u,v)}{\sigma_{Q}(u,v)}\\ \mathbf{Y}_{\mathcal{B}}(u,v) & -\dfrac{\sqrt{2}\sigma_{\mathcal{N}(\mathcal{B})}^{2}(u,v)}{\sigma_{Q}(u,v)}\le\bar{\mathbf{Y}}_{\mathcal{N}(\mathcal{B})}(u,v)-\mathbf{Y}_{\mathcal{B}}(u,v)\le\dfrac{\sqrt{2}\sigma_{\mathcal{N}(\mathcal{B})}^{2}(u,v)}{\sigma_{Q}(u,v)}\\ \bar{\mathbf{Y}}_{\mathcal{N}(\mathcal{B})}(u,v)+\dfrac{\sqrt{2}\sigma_{\mathcal{N}(\mathcal{B})}^{2}(u,v)}{\sigma_{Q}(u,v)} & \bar{\mathbf{Y}}_{\mathcal{N}(\mathcal{B})}(u,v)-\mathbf{Y}_{\mathcal{B}}(u,v)<-\dfrac{\sqrt{2}\sigma_{\mathcal{N}(\mathcal{B})}^{2}(u,v)}{\sigma_{Q}(u,v)}\end{cases} \quad (39)$$

ACKNOWLEDGMENT

The first author would like to thank Dr. Jiaying Liu for her work in revising the paper. He would like to also thank the three anonymous reviewers for their helpful comments and suggestions.

REFERENCES

[1] M.-Y. Shen and C.-C. Jay Kuo, "Review of Postprocessing Techniques for Compression Artifact Removal," *Journal of Visual Communication and Image Representation*, vol. 9, no. 1, pp.2-14, Mar. 1998.

[2] H.C. Reeve III and J.S. Lim, "Reduction of blocking effect in image coding," IEEE International Conference on Acoustics, Speech, and Signal Processing, vol.8, pp. 1212-1215, Apr. 1983.

[3] B. Ramamurthi and A. Gersho, "Nonlinear Space-variant Postprocessing of Block Coded Images," IEEE Trans. on Acoustics, Speech and Signal Processing, vol. 34, no. 5, pp. 1258-1268, Oct. 1986.

[4] A. Buades, B. Coll and J. M. Morel, "A Review of Image Denoising Algorithms, with A New One," *SIAM Journal on Multiscale Modeling and Simulation*, vol. 4, no. 2, pp.490-530, Jan. 2005.

[5] Antoni Buades , Bartomeu Coll , Jean-Michel Morel, "A Non-Local Algorithm for Image Denoising," IEEE international conference on Computer Vision Pattern Recognition, vol. 2, pp.60-65, Jun. 2005.

[6] H. Takeda, S. Farsiu, and P. Milanfar, "Kernel regression for image processing and reconstruction," *IEEE Trans. Image Processing*, vol. 16, no. 2, pp. 349–366, Feb. 2007.

[7] A. Zakhor, "Iterative Procedures for Reduction of Blocking Effects in Transform Image Coding," *IEEE Transl. on Circuits and Systems for Video Technology*, vol. 2, no. 1, pp.91-95, Mar. 1992.

[8] S. Minami and A. Zakhor, "An Optimization Approach for Removing Blocking Effects in Transform Image Coding," *IEEE Transl. on Circuits and Systems for Video Technology*, vol. 5, no. 2, pp.74-82, Apr. 1995.

[9] T.P. O'Rourke and R.L. Stevenson, "Improved image decompression for reduced transform coding artifacts," *IEEE trans. on Circuits and Systems for Video Technology*, vol. 5, no. 6, pp.490-499, Dec. 1995.

[10] D. Sun, W.-K. Cham, "Postprocessing of Low Bit-Rate Block DCT Coded Images Based on a Fields of Experts Prior," *IEEE Trans. Image Processing*, vol. 16, no. 11, pp. 2743–2751, Nov. 2007.

[11] S. Wu, H. Yan and Z. Tan, "An Efficient Wavelet-Based Deblocking Algorithm for Highly Compressed Images," *IEEE Transactions on Circuits and Systems for Video Technology*, vol. 11, no. 11, pp. 1193–1198, Apr. 2001.

[12] T. Chen, H.R. Wu and B. Qiu, "Adaptive Postfiltering of Transform Confidents for the Reduction of Blocking Artifacts," *IEEE Trans. on Circuits and Systems for Video Technology*, vol. 11, no. 5, pp. 594-602, May 2001.

[13] S. Liu and A. C. Bovik, "Efficient DCT-domain Blind Measurement and Reduction of Blocking Artifacts," *IEEE Trans. on Circuits and Systems for Video Technology*, vol.12, no.12, pp.1139-1149, Dec. 2002.

[14] S. S. O. Choy, Y.-H. Chan and W.-C. Siu, "Reduction of Block-transform Image Coding Artifacts by Using Local Statistics of Transform Coefficients," *IEEE Signal Processing Letters*, vol. 4, no. 1, pp. 5-7, Jan. 1997.

[15] K. Lee, D.S. Kim and T. Kim, "Regression-based Prediction for Blocking Artifact Reduction in JPEG-Compressed Images," *IEEE Trans. on Image Processing*, vol. 14, no. 1, pp. 36-48, Jan. 2005.

[16] A. Foi, V. Katkovnik and K. Egiazarian, "Pointwise Shape-Adaptive DCT for High-Quality Denoising and Deblocking of Grayscale and Color Images," *IEEE Trans. Image Process.*, vol. 16, no. 5, pp. 1395-1411, May 2007.

[17] D. K. Hammond and E. P. Simoncelli, "Image denoising with an orientation-adaptive Gaussian scale mixture model," IEEE Conference on Image Processing, Oct. 2006.

[18] M. F. Tappen, B. C. Russel, and W. T. Freeman, "Exploiting the sparse derivative prior for super-resolution and image demosaicing," in Proc. IEEE Workshop on Statistical and Computational Theories of Vision, 2003.

[19] T. S. Cho, N. Joshi, C. L. Zitnick, S. B. Kang, R. Szeliski and T. Freeman, "A content-Aware Image Prior," IEEE international conference on Computer Vision Pattern Recognition, 2010.

[20] S. Roth and M. Black, "Fields of Experts: A framework for learning image priors," IEEE international conference on Computer Vision Pattern Recognition, vol. 2, pp.860-867, 2005.

[21] W. Pennebaker and J. Mitchell, "JPEG Still Image Data Compression Standard," New York: Van Nostrand, 1993.

[22] J.L. Mitchell, W. B. Pennebaker, C. E. Fogg and D.J. LeGall, "MPEG Video Compression Standard," New York: Chapman & Hall, 1997.

[23] T. Wiegand, G. J. Sullivan, Gisle Bjøntegaard and A. Luthra, "Overview of the H.264/AVC Video Coding Standard," *IEEE Trans. on Circuits and Systems for Video Technology,* vol.13, no.7, pp.560-576, Jul. 2003.

[24] M. Robertson and R. Stevenson, "DCT Quantization Noise in Compressed Images," *IEEE Trans. on Circuits Systems for Video Technology*, vol.15, no.1, pp.27-38, Jan. 2005.
[25] B. K. Gunturk, Y. Altunbasak and R. Mersereau, "Superresolution Reconstruction of Compressed Video Using Transform-domain Statistics," *IEEE Trans. on Image Processing*, vol.13, no. 1, pp. 33-43, Jan. 2004.
[26] R.M. Gray and D. L. Neuhoff "Quantization," *IEEE Trans. on Information Theory*, vol.44, no. 6, Oct. 1998.
[27] Billingsley, Patrick, "Probability and Measure (Third ed.)," John Wiley & sons, 1995.
[28] K. Dabov, A. Foi, V. Katkovnik and K. Egiazarian, "Image Denoising by Sparse 3-D Transform-Domain Collaborative Filtering," *IEEE Trans. on Image Processing*, vol.16, no.8, pp. 2080-2095, Aug. 2007
[29] G. Zhai, W. Zhang, X. Yang, W. Lin and Y. Xu, "Efficient Image Deblocking Based on Postfiltering in Shifted Windows," *IEEE Transl. on Circuits and Systems for Video Technology*, vol. 18, no.1, pp.122-126, Jan. 2008.
[30] Aria Nosratinia, "Enhancement of JPEG-Compressed Image by Re-application of JPEG," *Journal of VLSI Signal Processing,* vol. 27, pp. 69-79, 2001
[31] M. Elad and M. Aharon, "Image Denoising Via Sparse and Redundant Representations Over Learned Dictionaries," *IEEE Trans. on Image Processing*, vol.15, no.12, pp. 3736-3745, Dec. 2006.
[32] P. Chatterjee and P. Milanfar, "Patch-Based Near-Optimal Image Denoising," *IEEE Trans. on Image Processing*, vol.21, no.4, pp. 1635-1649, Apr. 2012.
[33] JPEG Encoder and Decoder download from: http://www.ijg.org/.
[34] Z. Wang, A.C. Bovik, H.R. Sheikh and E.P. Simoncelli, "Image Quality Assessment: From Error Visibility to Structural Similarity," *IEEE Trans. on Image Processing*, vol. 13, no. 4, pp. 600-612, Apr. 2004.
[35] P. List, A. Joch, J. Lainema, G. Bjøntegaard and Marta Karczewicz, "Adaptive Deblocking Filter," *IEEE Trans. on Circuits and Systems for Video Technology*, vol. 13, no. 7, Jul. 2003.
[36] The H.264/AVC reference software is available from: http://iphome.hhi.de/suehring/tml/download/old_jm/.
[37] S. Farsiu, M. D. Robinson, M. Elad and P. Milanfar, "Fast and robust multiframe super-resolution," *IEEE Trans. Image Process.*, vol. 13, no. 10, pp.1327 -1344, 2004.
[38] E. Y. Lam and J. W. Goodman, "A mathematical analysis of the DCT coefficient distributions for images," *IEEE Trans. Image Process.*, vol. 9, no. 10, pp.1661-1666, 2000.

Xinfeng Zhang received the B.S. degree in computer science from Hebei University of Technology, Tianjin, China, in 2007. He is currently working toward the Ph.D. degree from the Institute of Computing Technology, Chinese Academy of Sciences, Beijing.

His current research interests include image and video processing, image and video compression.

Ruiqin Xiong (M'08) received B.S. degree from the University of Science and Technology of China, Hefei, China, in 2001, and the Ph.D. degree from the Institute of Computing Technology, Chinese Academy of Sciences, Beijing, China, in 2007.

He was with Microsoft Research Asia as a Research Intern from 2002 to 2007 and the University of New South Wales, New South Wales, Australia, as a Senior Research Associate, from 2007 to 2009. He joined Peking University, Beijing, in 2010. His current research interests include image and video compression, image and video restoration, joint source channel coding, and multimedia communication.

Xiaopeng Fan (S'07-M'09) received the B.S. and M.S. degrees from the Harbin Institute of Technology (HIT), China, in 2001 and 2003 respectively, and the Ph.D degree from Hong Kong University of Science and Technology (HKUST) in 2009.

In 2009, he joined the Department of Computer Science, Harbin Institute of Technology (HIT), where he is currently an Associate Professor. From 2003 to 2005, he worked with Intel China Software Laboratory (ICSL) as Software Engineer.

His current research interests are in image/video coding and processing, video streaming and wireless communication. He has authored or co-authored over 50 technical journal and conference papers.

Siwei Ma (M'12) received the B.S. degree from Shandong Normal University, Jinan, China, in 1999, and the Ph.D. degree in computer science from Institute of Computing Technology, Chinese Academy of Sciences, Beijing, China, in 2005.

From 2005 to 2007, he was a Post-Doctorate with the University of Southern California. Then he joined the Institute of Digital Media, EECS, Peking University, where he is currently an Associate Professor. He has published over 100 technical articles in refereed journals and proceedings in the areas of image and video coding, video processing, video streaming, and transmission.

Wen Gao (M'92–SM'05–F'09) received the Ph.D. degree in electronics engineering from the University of Tokyo, Tokyo, Japan, in 1991.

He is currently a Professor of computer science with the Institute of Digital Media, School of Electronic Engineering and Computer Science, Peking University, Beijing, China. Before joining Peking University, he was a Professor of computer science with the Harbin Institute of Technology, Harbin, China, from 1991 to 1995, and a Professor with the Institute of Computing Technology, Chinese Academy of Sciences, Beijing. He has published extensively including five books and over 600 technical articles in refereed journals and conference proceedings in the areas of image processing, video coding and communication, pattern recognition, multimedia information retrieval, multimodal interfaces, and bioinformatics.

Prof. Gao served or serves on the editorial boards for several journals, such as the IEEE TRANSACTIONS ON CIRCUITS AND SYSTEMS FOR VIDEO TECHNOLOGY, IEEE TRANSACTIONS ON MULTIMEDIA, IEEE TRANSACTIONS ON AUTONOMOUS MENTAL DEVELOPMENT, *EURASIP Journal of Image Communications, and Journal of Visual Communication and Image Representation*. He has chaired a number of prestigious international conferences on multimedia and video signal processing, such as IEEE ICME and ACM Multimedia, and also served on the advisory and technical committees of numerous professional organizations.